Supporting Information

"Delocalized π-bonds" Guided Pyramidal Nanocrystal Superstructures for Excellent Light Trapping in SERS

Yang Shang,[a] Bo Ren,[a] Xiaotian Wang,*[c] and Jie Lin*[b]

a Key Laboratory of Advanced Functional Materials, Ministry of Education, College of Materials Science and Engineering, Beijing University of Technology, Beijing, 100124, P. R. China

b Ningbo Institute of Materials Technology and Engineering, Chinese Academy of Science, 1219 Zhongguan West Road, Ningbo, 315201 China

Email: linjie@nimte.ac.cn

c School of Chemistry, Beijing Advanced Innovation Center for Biomedical Engineering, Key Laboratory of Bio-Inspired Smart Interfacial Science and Technology, Beihang University, Beijing100191, China

Email: wangxt@buaa.edu.cn

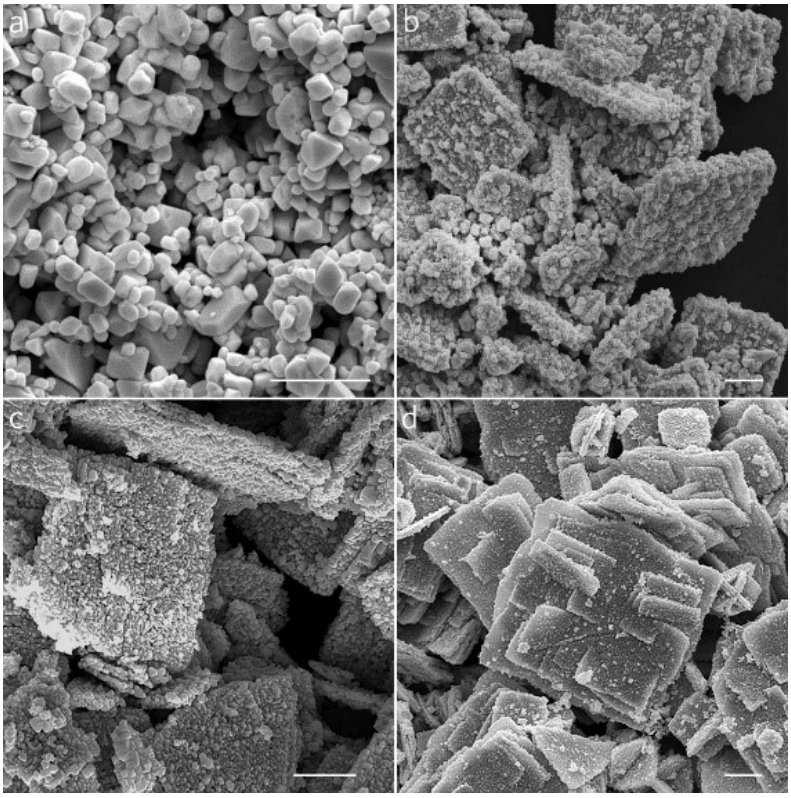

Fig. S1 SEM images of CuI samples obtained with different I^- concentrations. Scale bar = 2 μm. (a) 0.0089, (b) 0.0178, (c) 0.0268 and (d) 0.0357 M.

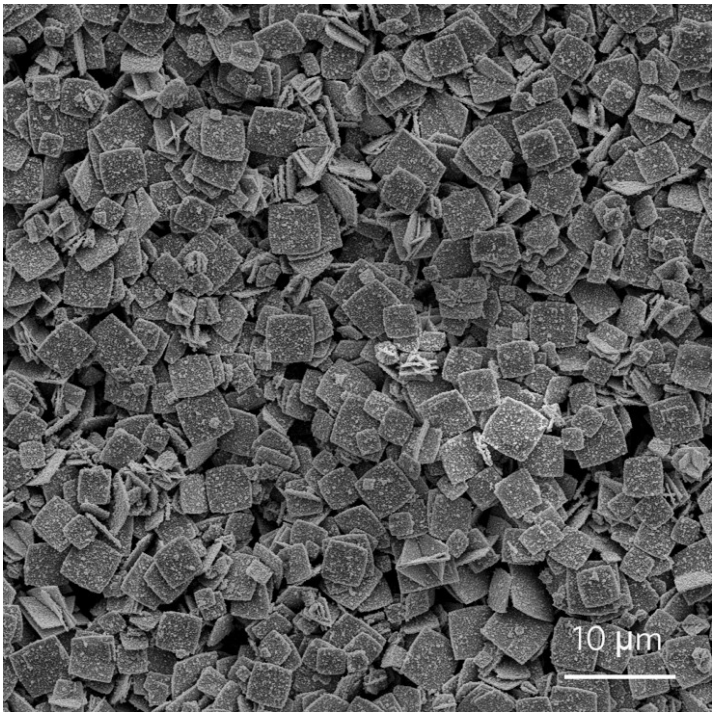

Fig. S2 Broad view SEM image of the CuI superstructure.

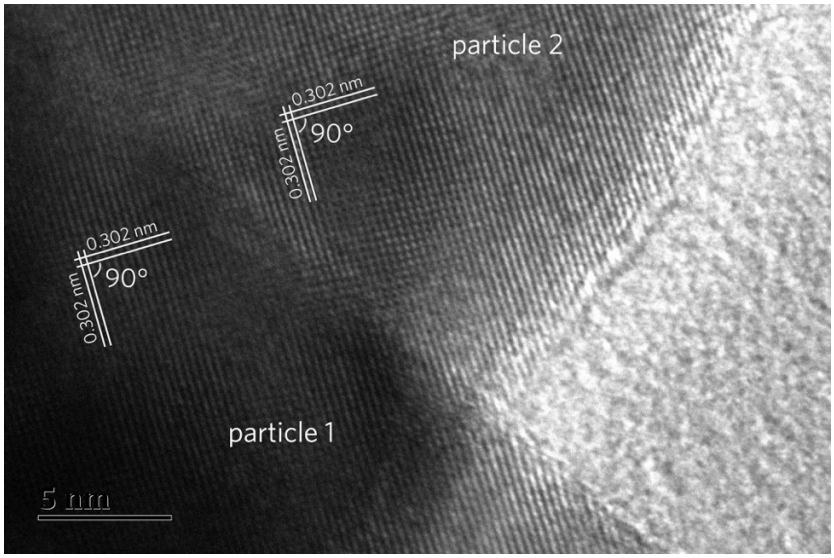

Fig. S3 The overall HRTEM image of Fig. 2f. The image demonstrated the identical crystallographic orientations of adjacent CuI quasi-octahedra.

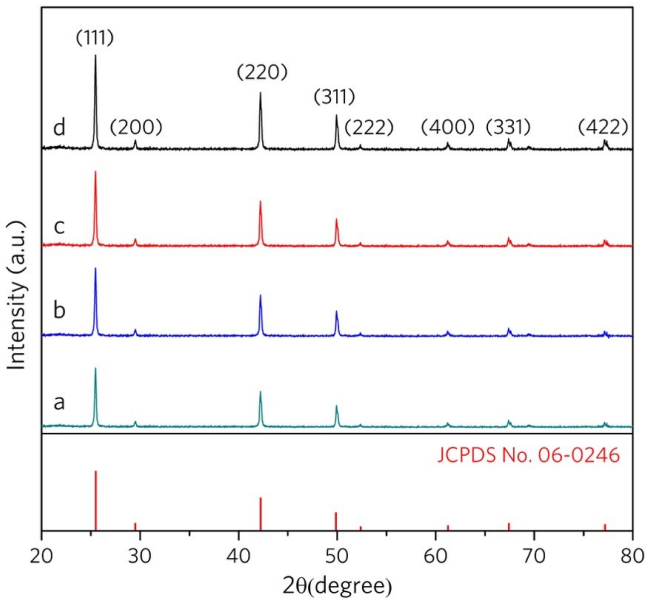

Fig. S4 (a~c) XRD patterns of the intermediates during the growth of the CuI superstructures collected at different duration time: (a) 0 min, (b) 30 min, (c) 60 min and (d) XRD pattern of the as-synthesized CuI superstructure with reaction for 120 min. All the products can be well indexed to the standard data for cubic CuI with JCPDS No. 06-0246.

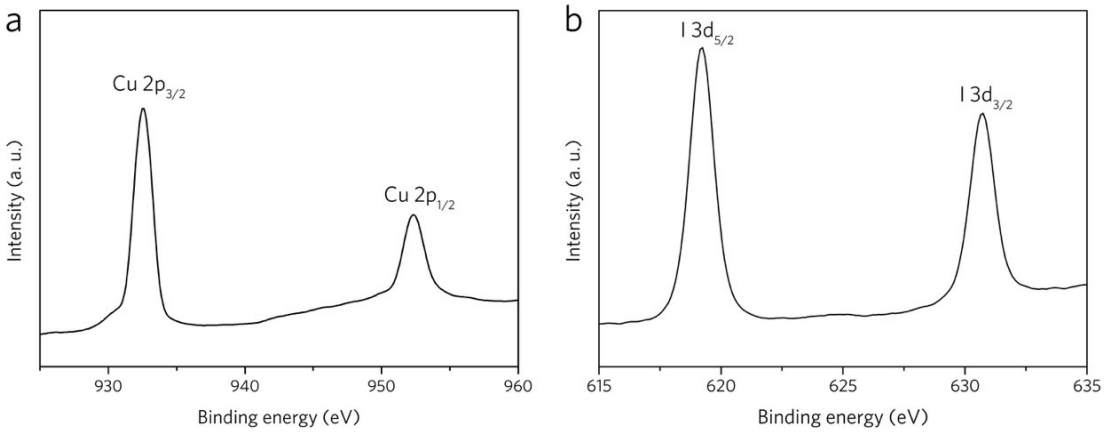

Fig. S5 XPS spectra of the as-prepared samples of CuI. It is observed that two strong peaks at 932.1 and 952.0 eV in Cu *2p* spectrum, and two strong peaks at 619.5 and 952.0 eV in I *3d* spectrum.

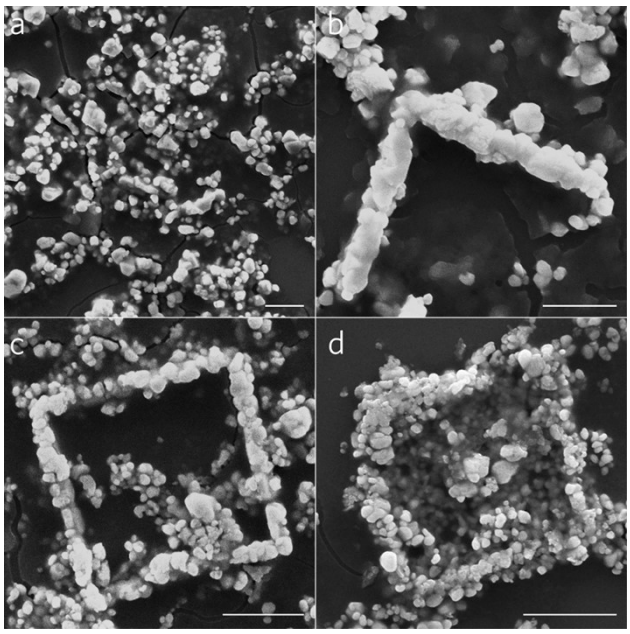

Fig. S6 SEM image of the intermediates during the growth of the CuI superstructures collected at different duration time: (a) 0, (b) 30, (c) 60 and (d) 90 min.

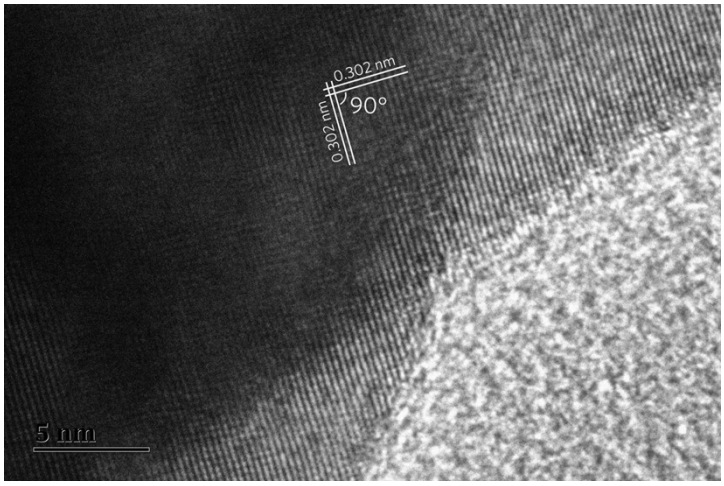

Fig. S7 The HRTEM image of boundary region in the red frame of Fig. 3b1. It showed a vertical set of lattice fringes of 0.302 nm for CuI quasi-octahedron subunit, which coincident well with the (200) plane of the cubic CuI. Remarkably, the identical crystallographic orientations on the edges of adjacent CuI quasi-octahedra (Fig. 3b1) suggested the uniform crystallographic orientations of the CuI frame.

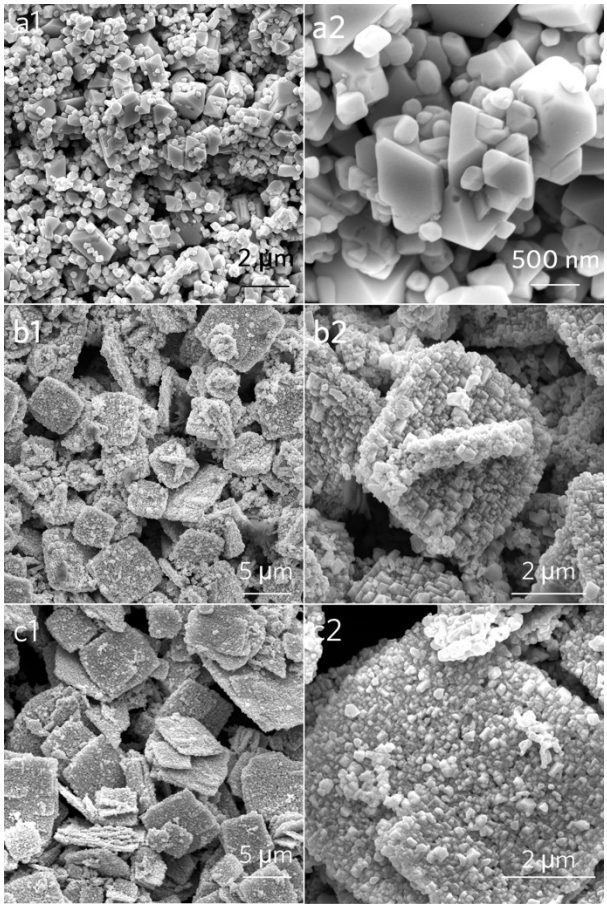

Fig. S8 SEM images of CuI samples obtained with different P123 concentrations. (a1, a2) 0, (b1, b2) 0.1, and (c1, c2) 0.4 M.

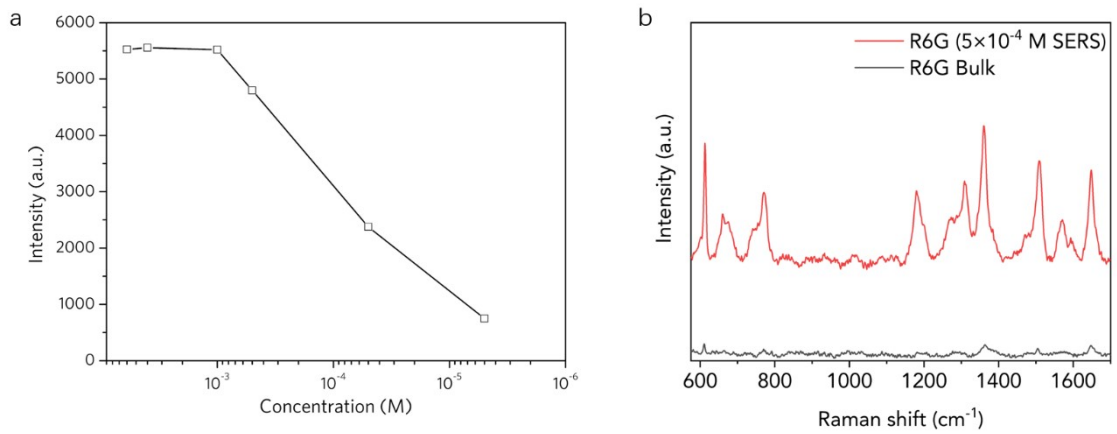

Fig. S9 (a) The relationship of peak intensities at 610 cm^{-1} and concentrations of R6G adsorbed on CuI superstructure single particle. (b) Black line is normal Raman spectrum of solid R6G, red line is SERS spectrum of R6G (5×10^{-4} M) adsorbed on CuI superstructure single particle. Laser wavelength: 647 nm; power: 3.0 mW; lens: 50 × objective; acquisition time: 2 s.

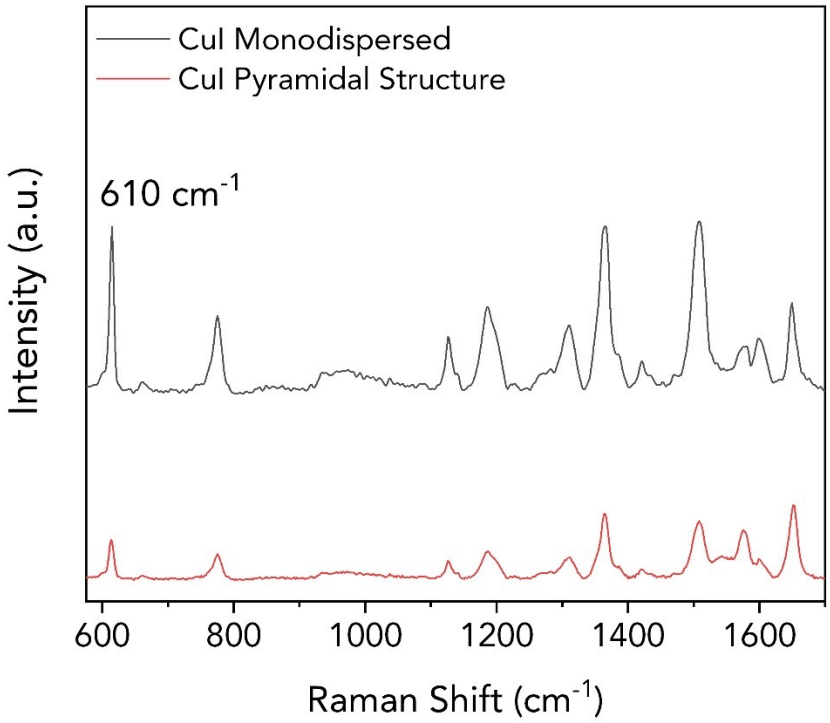

Fig. S10 SERS of R6G spectra (10^{-4} M) adsorbed on CuI superstructure and monodispersed octahedra by 647 nm excitation wavelength.

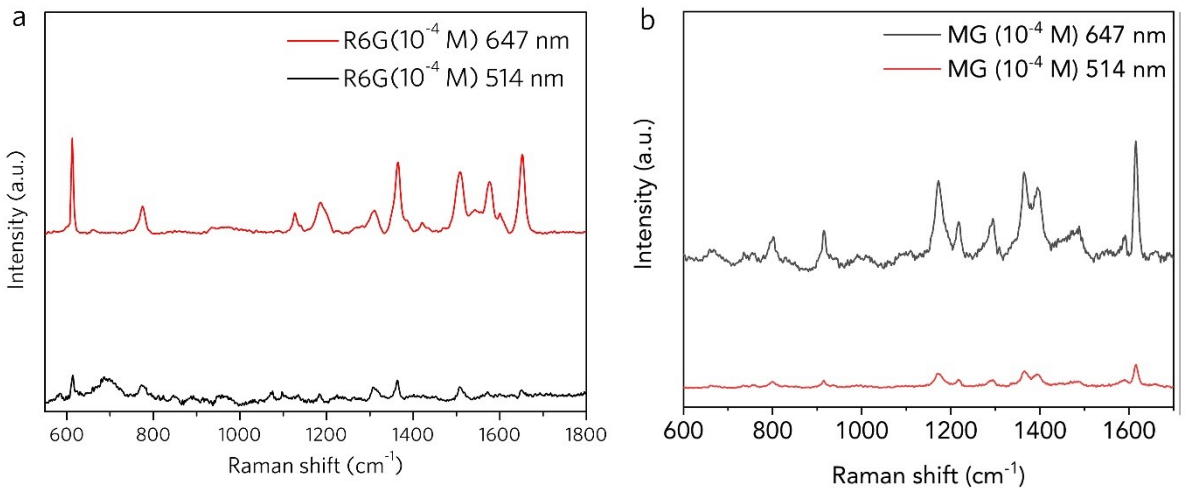

Fig. S11 (a) SERS of R6G spectra (10^{-4} M) adsorbed on CuI superstructure single particle by 514.5 nm excitation wavelength (black line) and 647 nm excitation wavelength (red line). (b) SERS of MG spectra (10^{-4} M) adsorbed on CuI superstructure single particle by 514.5 nm excitation wavelength (red line) and 647 nm excitation wavelength (black line).

The SERS spectra of R6G and MG (10^{-4} M) adsorbed on CuI superstructure by 647 nm laser was obviously better than that of 514.5 nm under the same condition.

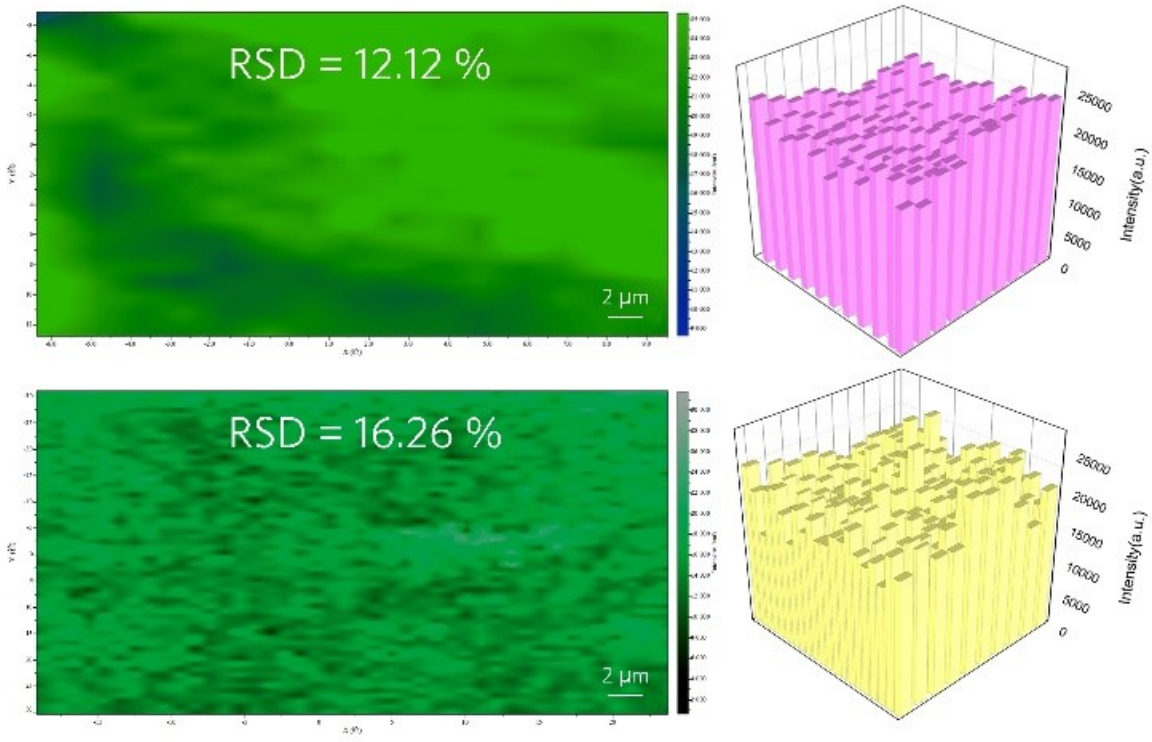

Fig. S12 Raman mapping images of the main vibration modes (a) R6G at 610 cm^{-1} and (c) MG at 1170 cm^{-1} recorded on a 30 × 30 μm area, and the corresponding intensity of the peaks in the area spots, respectively. The concentrations of R6G and MG is 10^{-4} M.

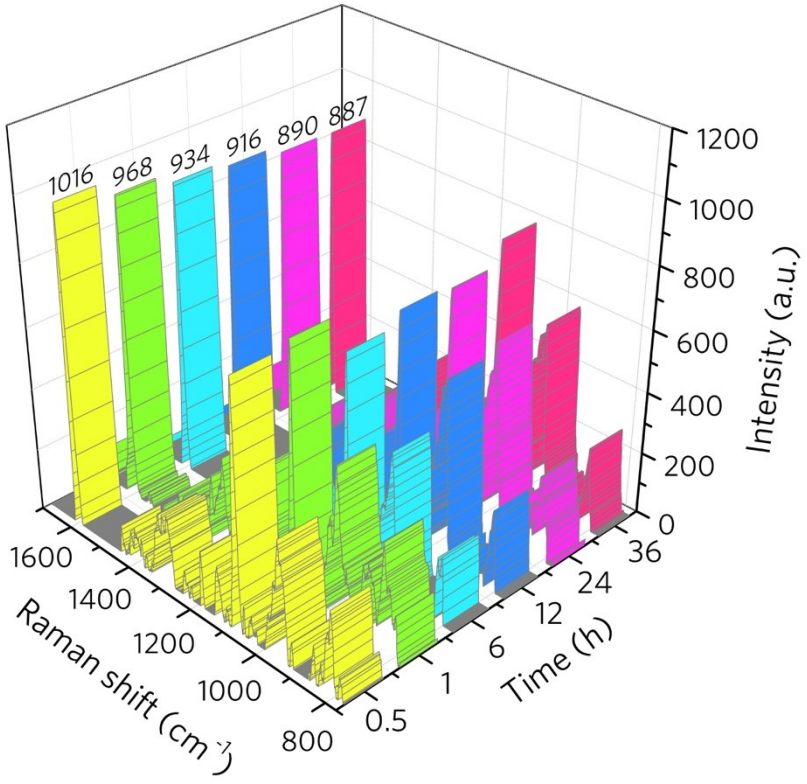

Fig. S13 Raman mapping images of the main vibration modes (a) R6G at 610 cm^{-1} and (c) MG at 1170 cm^{-1} recorded on a 30 × 30 μm area, and the corresponding intensity of the peaks in the area spots, respectively. The concentrations of R6G and MG is 10^{-4} M.

Supplementary Table 1: Comparing with semiconductors and noble metals SERS activity by literatures.

Materials	Analyte	EF	LOD (M)	Laser (nm)	Ref
CuI Pyramidal Structures	CV	2.8×10^5	10^{-7}	647	This work
H-Si nanowire/ H-Ge nanotube	R6G/N719	8-28	10^{-6}	532	Ref[1]
TiO_2 microarrays	Methylene Blue	2×10^4	6×10^{-6}	532	Ref[2]
TiO_2 nanoparticles	Dopamine	10^3	4×10^{-2}	442	Ref[3]
Cu_2O nanospheres	4-MBA	10^5	10^{-3}	488	Ref[4]
Cu_2O nanostructure	4-ATP	3.5×10^4	10^{-7}	532	Ref[5]
ZnO Superstructures	4-MPY	10^5	-	532	Ref[6]
WS_2	R6G	2.5×10^4	10^{-7}	532	Ref[7]
Partially oxidized MoS_2	R6G	1.4×10^5	10^{-7}	532	Ref[7]
Li-MoS_2	R6G	1.73×10^4	10^{-7}	532	Ref[8]
Amorphous Rh_3S_6	R6G	1.02×10^5	10^{-7}	647	Ref[9]
few-layer MoS_2	R6G	7.68×10^2	10^{-8}	532	Ref[10]
$Ni(OH)_2$ microcages	MB	2.35×10^3	10^{-7}	532	Ref[11]

Reference

[1] X. Wang, W. Shi, G. She, L. Mu, *J. Am. Chem. Soc.* **2011**, 133, 16518.

[2] D. Qi, L. Lu, L. Wang, J. Zhang, *J. Am. Chem. Soc.* **2014**, 136, 9886.

[3] A. Musumeci, D. Gosztola, T. Schiller, N. M. Dimitrijevic, V. Mujica, D. Martin, T. Rajh, *J. Am. Chem. Soc.* **2009**, 131, 6040.

[4] L. Jiang, T. You, P. Yin, Y. Shang, D. Zhang, L. Guo, S. Yang, *Nanoscale* **2013**, 5, 2784.

[5] C. Qiu, L. Zhang, H. Wang, C. Jiang, *J. Phys. Chem. Lett.* **2012**, 3, 651.

[6] W. Ji, L. Li, W. Song, X. Wang, B. Zhao, Y. Ozaki, *Angew. Chem. Int. Ed.* **2019**, 58, 14452.

[7] Z. Zheng, S. Cong, W. Gong, J. Xuan, G. Li, W. Lu, F. Geng, Z. Zhao, *Nat. Commun.* **2017**, 8, 1993.

[8] E. Er, H.-L. Hou, A. Criado, J. Langer, M. Möller, N. Erk, L. M. Liz-Marzán, M. Prato, *Chem. Mater.* **2019**, 31, 5725.

[9] A. Li, J. Lin, Z. Huang, X. Wang, L. Guo, *iScience* **2018**, 10, 1.

[10] B. P. Majee, S. Mishra, R. K. Pandey, R. Prakash, A. K. Mishra, *J. Phys. Chem. C* **2019**, 123, 18071.

[11] M. Gao, P. Miao, X. Han, C. Sun, Y. Ma, Y. Gao, P. Xu, *Inorg. Chem. Front.* **2019**, 6, 2318.